Revision 1

Behavior of hydrogen defect and framework of Fe-bearing wadsleyite and ringwoodite at high temperature and high pressure

Yang Jin[1], Weihua Huang[1], ZhongPing Wang[2], Wei Sun[3], Yan Liu[1], Qunke Xia[1], Yan Yang[1, *]

[1]Institute of Geology and Geophysics, School of Earth Sciences, Zhejiang University, Hangzhou 310027, China
[2]Department of Physics, University of Science and Technology of China, Hefei, Anhui 230026, China
[3]State Key Laboratory of Geological Processes and Mineral Resources, China University of Geosciences, Wuhan 430074, China
Corresponding author*
Institute of Geology and Geophysics
School of Earth Sciences
Zhejiang University
Hangzhou 310027, China
Email: yanyang2005@zju.edu.cn

ABSTRACT

The transition zone is dominated by polymorphs of olivine, wadsleyite and ringwoodite, which are to date considered the main water carriers in the Earth's mantle. Despite considerable efforts on water solubility and impact on physical properties of the two minerals, knowledge of hydrogen defects and framework behavior of the two minerals at high temperature and high pressure is still lacking. Here, we systematically assess this issue, by *in situ* high temperature (20-800 °C) infrared spectroscopic, *in situ* high temperature (20-800 °C) and high temperature-pressure (14.27 GPa and 18.84 GPa, 20-400 °C) Raman spectroscopic studies on the iron-bearing wadsleyite and ringwoodite. The results show that dehydrogenation in wadsleyite happens at a higher temperature than in ringwoodite. The infrared absorption patterns of hydrogen defects in wadsleyite and ringwoodite are temperature sensitive, resulting from hydrogen defects transferring and site-specific stabilities. As for the framework, it is more sensitive to temperature and pressure for the ringwoodite than the wadsleyite. These results provide new knowledge about hydrogen defects and framework of wadsleyite and ringwoodite at high temperature and high pressure, which is indispensable for understanding water solubility and its impacts on physical properties of the two minerals.

Keywords: wadsleyite; ringwoodite; hydrogen defect; framework; mantle transition zone

INTRODUCTION

Many geochemical and mineralogical studies have contributed to water distribution in the mantle transition zone. However, there still exist uncertainties. Based on the crystallographic considerations and experimental estimation of hydrogen solubility (Smyth, 1994; Kohlstedt et al., 1996), the mantle transition zone can be a large water reservoir, with up to 2.7 wt.% H_2O in the structures of wadsleyite and ringwoodite. But this is inconsistent with the geophysical observation which suggests less water in the mantle transition zone (Houser, 2016). However, a single natural ringwoodite, found in a diamond, contains about 1.4 wt.% H_2O (Pearson et al., 2014), and thus clearly demonstrated at least locally a water-rich mantle transition zone. Moreover, hydrogen effects on physical properties of wadsleyite and ringwoodite have been extensively studies. However, large discrepancies exist about the magnitude of hydrogen effects among different studies (e.g., Huang et al., 2005; Yoshino et al., 2008a, 2008b; Yoshino and Katsura, 2012; Dai and Karato, 2014). Hydrogen impacts on some physical properties are even different between wadsleyite and ringwoodite. For example, hydrogen has a larger effect on electrical conductivity and elastic property of ringwoodite than on the same properties of wadsleyite, while hydrogen has a smaller effect on thermal expansion and Fe-Mg interdiffusion in ringwoodite than in wadsleyite (Zhang and Xia 2021 and references therein). But the physical mechanisms are unclear.

To understand the water storage and its impacts on physical properties of the mantle transition zone, it is necessary to reveal behavior of hydrogen defects and framework of the two minerals at high temperature and high pressure. The temperature of dehydrogenation has been previously inferred from the thermal expansion experiments, to be 450 °C-362 °C for wadsleyite (Ye et al., 2009; Inoue et al., 2014; 2011), and 400 °C-313 °C for ringwoodite (Ye et al., 2011; Inoue et al., 2014). Although hydrogen diffusivity in wadsleyite has been fitted through the annealing experiments at high temperatures and high pressures (Hae et al., 2006), it is not dehydrogenation by ionic diffusion. Only one study performed molecular

dynamics simulations and determined hydrogen diffusivities in wadsleyite and ringwoodite (Caracas and Panero, 2017), and experimental evidence about hydrogen mobilities in the two minerals is lacking. Infrared spectroscopy is an efficient method for clarify hydrogen defects in minerals. However, current knowledge about hydrogen defects in wadsleyite and ringwoodite has been based mainly on infrared spectra at room or low temperature at high pressure (Chamorro Pérez et al., 2006; Deon et al., 2010; Koch-Müller et al., 2011; Panero et al., 2013). To date, only two studies have reported infrared spectra of hydrogen defects at high temperatures. Mrosko et al. (2013) reported infrared spectra of an Fe-bearing ringwoodite at high temperatures to 600 °C. Yang et al. (2014) reported infrared spectra of wadsleyite and ringwoodite at simultaneously high temperature and high pressure, but the samples used are Fe-free. In the same case, there have been few reports on framework behavior of wadsleyite and ringwoodite, but mainly under high pressures at ambient temperature (Liu et al., 1998, 2002; Kleppe et al., 2001, 2002a, 2002b, 2006). Only one study reported the lattice vibrations of wadsleyite at simultaneous high temperature and high pressure (Yang et al., 2012), but the sample is Fe-free and a possible Fe impact is unknown.

In this study, we perform experiments to assess hydrogen defect and framework behavior in the Fe-bearing wadsleyite and ringwoodite using *in situ* infrared spectroscopic (IR) and Raman spectroscopic at high temperatures and high pressures. Complementary with previous studies on Fe-free samples, the results may promote further understanding of hydrogen defect and framework of wadsleyite and ringwoodite.

EXPERIMENTAL METHODS

Sample description

The samples used in this study are iron-bearing hydrous wadsleyite and ringwoodite single crystals, which were synthesized by Sun et al. (2015, 2018), using a Kawai-Type Multianvil Apparatus. The iron-bearing hydrous wadsleyite grains were synthesized from San Carlos olivine at 16 GPa and 1723K, with water content about 0.95 wt.% (Sun et al., 2018). The iron-bearing hydrous ringwoodite grains were synthesized at 21 GPa and 1723 K, by a slow cooling method, with San Carlos olivine as the starting material. The water content is about 0.77 wt.% (Sun et al., 2015). The

sample grains are with size range from 50 to 600 μm. The wadsleyite and ringwoodite crystals were polished to 20-25 μm thickness and 70-80 μm thickness, respectively, for infrared spectra measurements. Chemical compositions of the two samples were analyzed by an EMPA 1720H (Shimadzu) electron microprobe in this study. The accelerating voltage is 15 kV, the beam current is 20 nA and the beam diameter is 5 μm. The characteristic peak test time and background test time are both 10 s. Natural olivine was used as a standard for Si and Mg measurements, and natural pyrope was used as a standard for Fe measurement. The average chemical composition of wadsleyite is as following: 41.83 wt.% SiO_2, 50.59 wt.% MgO, 7.21 wt.% FeO; The average chemical composition of ringwoodite is as follows: 43.45 wt.% SiO_2, 48.50 wt.% MgO, 8.55 wt.% FeO. The standard deviations of all elements are less than 2 wt.%.

In situ Fourier transform infrared spectroscopy (FTIR)

The *in situ* infrared spectra were collected in the range of 4000-1000 cm^{-1} at elevated temperatures to 800 °C, using a Nicolet iS50 FTIR spectrometer coupled with a Continuum microscope at Zhejiang University (China). The spectrometer is equipped with a KBr beam splitter and an MCT-A (mercury cadmium telluride) detector cooled by liquid nitrogen. A total of 128 scans were accumulated for each spectrum at a 4 cm^{-1} resolution. The aperture size was set to 50-100× 50-100 μm. All IR measurements were carried out in a transmission mode. To generate high temperatures, an Instec HS1300 heating stage was attached to the microscope. The sample grain was placed on a sapphire plate in the heating stage with N_2 atmosphere. Two sets of experiments were performed: *in situ* heating and quench. For *in situ* heating, the temperature was raised from 20 °C to 800 °C at a heating rate of 15 °C/min. The infrared spectra were acquired at 20 °C, 100 °C, 200 °C, 300 °C, 400 °C, 500 °C, 600 °C, 700 °C and 800 °C and 20 °C quenched from 800 °C. The second heating experiment was carried out using the same experimental conditions as *in situ* heating. But the infrared spectra were collected on the quenched samples after every target temperature. The sample spectra at all temperatures were collected in the same area of the sample for each experiment, and the background spectra were collected at each temperature. The temperature uncertainty is less than 1 °C.

In situ high-temperature Raman spectroscopy

In situ Raman spectra were collected in the range of 1200-50 cm^{-1} using a LABRAM-HR Raman spectrometer at Zhejiang University (China). Single-crystal silicon was used as a reference. The sample was excited by the 532 nm green light. The diameter of the focused laser spot was estimated to be 1 μm. A ×50 objective was used to focus the incident laser light on the sample and to collect the scattered light. The high temperature was generated by an Instec HP1500G heating stage. The sample was heated with a rate of 15 °C/min from room temperature to 100 °C, 200 °C, 300 °C, 400 °C, 500 °C, 600 °C, 700 °C and 800 °C, respectively. At each temperature step, the Raman spectrum was collected on the same area of the sample.

In situ high-temperature and high-pressure Raman spectroscopy

In situ Raman spectra in the range of 1200-50 cm^{-1} at simultaneously high temperature and high pressure were collected using a HORIBA T64000 Raman spectrometer at the University of science and technology of China. The sample was excited by the 532 nm green light. The diameter of the focused laser spot was estimated to be 1.5 μm. A symmetric piston-cylinder-type diamond-anvil cell (DAC) with an external resistive heater was used to generate high temperature and high pressure. The size of the diamond culet is 400 μm. A 150 μm diameter hole was drilled into the stainless steel (t301) gasket. The sample chamber was filled with KBr powder and ruby chips for pressure-transmitting medium and pressure calibration, respectively. Two loadings were prepared for each mineral: one for compression to high pressure at room temperature and the other one for heating to high temperature at a constant pressure (~14.27 GPa for wadsleyite and ~18.84 GPa for ringwoodite). In the high-temperature runs, the resistive heater was placed inside the DAC and around the gasket between the diamond anvils (in air), and a K-type thermocouple was used to estimate temperature. The sample was heated to 100 °C, 200 °C, 300 °C and 400 °C, respectively at a heating rate of 10 °C/min. The pressure prior to and after each Raman spectrum measurement was determined by ruby fluorescence with a HORIBA T64000 spectrometer as calibrated for hydrostatic conditions by Mao et al. (1986) and Rekhi et al. (1999). For each measurement, the variation of pressure was <0.2 GPa and the variation of temperature was <1 °C as recorded by the K-type thermocouple.

RESULTS

Characteristics of hydrogen defects in the Fe-bearing wadsleyite and ringwoodite at ambient condition

Due to the anisotropy of wadsleyite, we used the polarized infrared spectroscopy for the measurements on the randomly oriented wadsleyite. On the contrary, only unpolarized infrared spectroscopy was applied on the cubic and isotropic ringwoodite. Typical spectra acquired at ambient condition are shown in Figure 1. There are two groups of OH bands for wadsleyite with wavenumbers higher and lower than 3500 cm^{-1}, respectively: 3612, 3583, 3385 and 3335 cm^{-1} (Fig. 1a). The OH bands wavenumbers are similar to those of the iron-free wadsleyites reported by previous studies (e.g., Jacobsen et al., 2005; Kohn et al., 2002; Deon et al, 2010; Yang et al., 2014). Therefore, iron seems has little effect on O-H bonding strength at ambient condition. But the prominent OH peak at 3612 cm^{-1} is consistent with previous studies showing that trivalent iron in wadsleyite can increase intensities of the 3611 cm^{-1} peak (e.g., Bolfan-Casanova et al., 2012). The polarized infrared spectra of wadsleyite in Figure 1a indicate that the O-H dipole corresponding to the 3612 cm^{-1} band orients differently to those corresponding to the 3583, 3385 and 3335 cm^{-1} bands, suggesting different hydrogen sites yet still poorly constrained. According to Jacobsen et al. (2005), the 3612 cm^{-1} and 3583 cm^{-1} peaks were assigned to bending hydrogen bonding along O1...O3 edge of M3, but located on two mutually perpendicular a-c and b-c planes, respectively. The main peaks at 3385 cm^{-1} and 3335 cm^{-1} were assigned to hydrogen bonding along O1...O4 edge of M3 or along the shared O1...O4 edge of M3 and M2 (Jacobsen et al., 2005), but the evidence from high-pressure infrared spectroscopy excludes the latter (Deon et al., 2010). The degree of hydrogen disordering in wadsleyite has been found to increase with an increasing of water content (Kohn et al., 2002), which further complicates hydrogen sites in wadsleyite if place in the conditions of a hydrogen-rich mantle transition zone. The polarization behavior of OH bands in our study suggest at least two groups of hydrogen sites in this Fe-bearing wadsleyite sample.

Consistent with the previous reported OH bands patterns in ringwoodite (Bolfan-Casanova et al., 2000; Chamorro Pérez et al., 2006; Panero et al., 2013; Yang et al., 2014; Fei and Katsura, 2020; Thomson et al., 2021), the unpolarized infrared spectrum of ringwoodite shows three groups of OH bands: a weak band at 3700-3600

cm^{-1}, a broad band centering at 3125 cm^{-1} ranging from 3600 to 2700 cm^{-1}, and a weak band at 2700-2500 cm^{-1} (Fig. 1b). Band deconvolution results further show that there are at least seven OH peaks at 3650, 3425, 3307, 3125, 2890, 2666, 2537 and 2443 cm^{-1} as shown in Figure 1b. In contrast to the general hydrogen substitution for Mg^{2+} vacancies in wadsleyite, hydrogen incorporation mechanism in ringwoodite is less constrained by point defect theory. For ringwoodite, multiple hydrogen incorporation mechanisms have been proposed. The weak band at 3700-3600 cm^{-1} was assigned to hydrogen associated with tetrahedral vacancies, the extremely broad band at 3600-2700 cm^{-1} could belong to disordered hydrogen associated with octahedral vacancies, and the weak band at 2700-2500 cm^{-1} was attributed to hydrogen associated with disordered silicon in octahedron (Chamorro Pérez et al., 2006; Mrosko et al., 2013; Panero et al., 2013; Grüninger et al., 2017; Thomson et al., 2021). Specifically, the 3400-3425 cm^{-1} band was assigned to ferric iron disorder onto the tetrahedral site (Thomson et al., 2021). Especially, previous studies revealed some differences in OH spectra feature between Fe-bearing and Fe-free ringwoodite. For example, an increase in iron content in ringwoodite, induced a drift of the OH peak from the higher wavenumber region to the lower wavenumber region, while the OH peak in the lower wavenumber region moves to the higher wavenumber region (Mrosko et al., 2013). Indeed, the peak position in the higher wavenumber region of our studied Fe-bearing ringwoodite is 3650 cm^{-1}, lower than 3695 cm^{-1} and 3668 cm^{-1} observed in the Fe-free ringwoodite (Chamorro Pérez et al., 2006; Yang et al., 2014). In addition, the resolved 3425 cm^{-1} peak here matches the Fe-bearing sample as well.

FTIR spectra of hydrogen defects in the wadsleyite and ringwoodite with increasing temperature

Figure 2 shows infrared spectra of hydrogen defects in the Fe-bearing wadsleyite and ringwoodite collected at the target temperatures and room temperature quenched from every target temperature. The OH bands almost disappear with temperature reaching 700 °C and 800 °C for the wadsleyite and ringwoodite, respectively (Fig. 2a-c). In addition, the spectra patterns change a lot with increasing temperature above 300 °C for the wadsleyite and 500 °C for the ringwoodite. The intensity of OH peak at 3335 cm^{-1} of wadsleyite greatly decreases, while the intensities of OH peaks at 3583 cm^{-1} and 3385 cm^{-1} increase. These variations appear in both the polarized spectra

along two perpendicular directions (Fig. 2a-b), excluding the possible temperature-induced change of O-H dipole direction. For ringwoodite, the broad band at 3600-2700 cm^{-1} converges to the high-wavenumber region, which is in agreement with the previous observation for an Fe-bearing ringwoodite (Mrosko et al., 2013). These changes are irreversible as shown in the spectra of the quenched samples (Fig. 2d-f).

Raman modes of the wadsleyite and ringwoodite at ambient condition

The Raman spectra of the wadsleyite and ringwoodite at ambient condition are shown in Figure 3, which is roughly consistent with previous reports except several differences. The Raman spectra of wadsleyite show six groups of Raman modes, which are located at 173 cm^{-1}, 543 cm^{-1}, 616 cm^{-1}, 720 cm^{-1}, 778 cm^{-1} and 918 cm^{-1} respectively. According to previous mode assignments (e.g., Mernagh and Liu., 1996), the mode at 173 cm^{-1} belongs to the lattice vibrations, the mode at 543 cm^{-1} belongs to the combination of SiO_3 and MgO_6 vibrations, the mode at 616 cm^{-1} belongs to the bending vibration of SiO_3, the mode at 720 cm^{-1} belongs to the symmetrical stretching vibration of Si_2O_7, and the mode at 918 cm^{-1} is generated by the symmetrical stretching of SiO_3. The Raman spectra of ringwoodite show the Raman modes at 93 cm^{-1}, 211 cm^{-1}, 237 cm^{-1}, 300 cm^{-1}, 326 cm^{-1}, 371 cm^{-1}, 414 cm^{-1}, 490 cm^{-1}, 596 cm^{-1}, 797 cm^{-1} and 838 cm^{-1} respectively. The modes at 237 cm^{-1}, 300 cm^{-1}, 371 cm^{-1}, 596 cm^{-1}, 797 cm^{-1} and 838 cm^{-1} are in agreement with previous reports (Chopelas et al., 1994; Kleppe et al., 2002a, 2002b; Liu et al., 2002). The two main modes at 797 cm^{-1} and 838 cm^{-1} belong to the SiO_4 stretching vibrations.

Raman modes of the wadsleyite and ringwoodite at high temperatures and high pressures

The *in situ* high temperature Raman spectra of wadsleyite and ringwoodite at ambient pressure are shown in Figure 4a-b. For wadsleyite, several new peaks appear in the spectra from 200 °C to 400 °C at ambient pressure. Among them, the Raman mode at 1029 cm^{-1} was also reported in the pure Mg wadsleyite (Kleppe et al., 2001). In addition, the intensities of the original Raman peaks are also significantly enhanced in this temperature range. Therefore, these peaks appearing at 200 °C may not be additional modes but would be due to the signal strengthening. During the heating process from room temperature to 800 °C, there is no additional Raman modes

occurring, suggesting no phase transition in this temperature range. However, the Raman spectrum of wadsleyite changes significantly after being quenched from 800 °C, with several additional modes appearing. This indicates that wadsleyite may eventually have undergone phase transition during the whole process. For ringwoodite, the phase transition can be clearly indicated by the abrupt change of the spectrum at temperatures above 700 °C. Some new modes appear in the Raman spectrum after the sample being quenched from 800 °C, such as 855 cm^{-1}, 825 cm^{-1}, 697 cm^{-1}, 610 cm^{-1}, 473 cm^{-1} and 323 cm^{-1}. Among them, the 855 cm^{-1} and 825 cm^{-1} band are the characteristic modes of olivine. Therefore, ringwoodite may have transformed back to olivine when the temperature reaches 700 °C at ambient pressure. Previous studies suggested that the phase transition temperature of ringwoodite at ambient pressure depends on the sample size. They found that the phase transition occurred at 527 °C when the particle size was less than 50 μm, and the phase transition did not occur up to 550 °C when the particle size was greater than 50 μm (Liu et al., 2002). In our study, the phase transition temperature is above 700 °C, which is in accordant with the larger size of the grains in our study.

In order to explore the effect of pressure on the framework behavior at high temperatures, the *in situ* high temperature Raman spectra of wadsleyite and ringwoodite were measured at 14.27 GPa and 18.84 GPa, respectively, as shown in Figure 4c-d. When the pressure rises to the corresponding pressure of the mantle transition zone, e.g., 14.27 GPa for wadsleyite and 18.84 GPa for ringwoodite, the Raman modes of the two samples shift significantly to higher wavenumbers, compared with the Raman modes at ambient pressure. The shift amplitudes are larger for the ringwoodite than the wadsleyite. During the heating process at high pressure, no new mode was found, which is inconsistent with the observation of two new modes at 714 and 550 cm^{-1} appearing for pure Mg-wadsleyite heated to 400 °C at 14.5 GPa (Yang et al., 2012).

DISCUSSION

Behavior of hydrogen defects in the wadsleyite and ringwoodite with increasing temperature

In order to assess dehydrogenation of the two samples, we analyzed the OH

spectra of the samples at high temperatures and quenched from different temperatures. Figure 5 shows the evolutions of bulk integral absorbance of OH bands with temperature. The bulk integral absorbances display the similar trends between those obtained from the spectra at the target temperatures and room temperature after the target temperatures. For the wadsleyite, the bulk OH integral absorbance slightly decreases and reduces by 30% with increasing temperature to 600 °C, and then drastically decreases to almost zero at 800 °C. For the ringwoodite, the bulk OH integral absorbance decreases by 20% with increasing temperature to 400 °C, and greatly reduces to almost zero at 800 °C. The slight variations below 600 °C for the wadsleyite and 400 °C for the ringwoodite may be caused by the heating-induced O-H anharmonicity. In contrast, the absorbance subsequently decreases by 70% from 600 to 800 °C for the wadsleyite, and 80% from 400 to 800 °C for the ringwoodite. This significant reduction should be accounted by dehydrogenation. Therefore, the turning points of the OH absorbance evolutions reveal the dehydrogenation temperature of the two samples during the heating processes, that is 600 °C for the wadsleyite while 400 °C for the ringwoodite. The dehydrogenation temperatures of Fe-bearing wadsleyite and ringwoodite obtained in this study are higher than those of the Fe-free counterparts (Inoue et al., 2004; Ye et al., 2009, 2011, 2012). For example, based on the thermal expansion experiments, the dehydrogenation temperatures of wadsleyite were reported to be 450 °C (Inoue et al., 2004), 382 °C (Ye et al., 2009) and 362 °C (Ye et al., 2011), and the dehydrogenation temperatures of ringwoodite were suggested to be 400 °C (Inoue et al., 2004) and 313 °C (Ye et al., 2011). Fe may potentially be responsible for this difference. Indeed, no dehydrogenation occurs in the very recent work for the elastic property measurement at 427 °C (700 K) of a hydrous Fe-bearing wadsleyite (Zhou et al., 2022). Besides Fe, the difference may be caused by other factors, such as annealing duration, crystal or powder and even water content. Anyway, the results of our study and previous studies show that the dehydrogenation temperature of wadsleyite is higher than that of ringwoodite. In Inoue et al. (2011), the Fe-free wadsleyite dehydrogenation temperature is 50 °C higher than the Fe-free ringwoodite dehydrogenation temperature. In Ye et al. (2011), the dehydrogenation temperature of the Fe-free wadsleyite is 49 °C higher than that of the Fe-free ringwoodite. Coincidentally, the dehydrogenation temperature of the Fe-bearing wadsleyite is 200 °C higher than that of the Fe-bearing ringwoodite in this study.

These results experimentally confirm the different hydrogen mobilities between wadsleyite and ringwoodite previously proposed using molecular dynamics (Caracas and Panero, 2017). The contrast dehydrogenation temperature between wadsleyite and ringwoodite may indicate that hydrogenated lattice of ringwoodite is less stable than that of hydrogenated wadsleyite, which is further confirmed by their different framework responses to temperature and pressure. It should be noted that we provided the dehydrogenation temperatures of the wadsleyite and ringwoodite in this heating condition. It deserves to compare dehydrogenation of the two minerals at the pressure conditions of the mantle transition zone.

To clarify the variations of the OH spectra patterns with increasing temperature and dehydrogenation processes, the site-specific evolutions of OH integral absorbance in the wadsleyite and ringwoodite are displayed in Figure 6. For the wadsleyite, the integral absorbance ratios of 3583 to 3335 cm^{-1} band ($Ab_{3583/3335}$) and 3385 to 3335 cm^{-1} band ($Ab_{3385/3335}$) change with increasing temperature. At temperatures above 200 °C, the ratios significantly enhance with temperature, which could account for the OH spectra pattern changing shown in Figure 2. Since these changes occur at temperatures lower than the dehydrogenation temperature of 600 °C for the wadsleyite, the process should be attributed to possible transition between different hydrogen detects. Therefore, hydrogen defects responsible for the 3583, 3385 and 3335 cm^{-1} peaks may have different stabilities, and the hydrogen defects corresponding to the 3583 and 3385 cm^{-1} bands may be predominant before dehydrogenation. The results uncover the possible dehydrogenation process of wadsleyite, that is, protons may transfer and re-distribute locally in the lattice before dehydrogenation. It can also be noticed that the relative intensity of OH peaks in the Fe-bearing wadsleyite changes after heating at 423 °C (700 K) (Supplementary Fig. 6 in Zhou et al., 2022), which is consistent with the conclusion in our study. This dehydrogenation process involving hydrogen transferring was also suggested in olivine (e.g., Jollands et al., 2019)

For ringwoodite, the integral absorbance ratios of 3650 to 3125 cm^{-1} band ($Ab_{3650/3125}$) and 3425 to 3125 cm^{-1} band ($Ab_{3425/3125}$) drastically increase at temperatures above 400 °C, suggesting different stabilities of the hydrogen defects. That is, hydrogen defects responsible for the OH peaks at high-wavenumber region

are more stable than those at low-wavenumber region. This is also consistent with previous molecular dynamics simulations that hydrogen defects related to octahedral vacancies diffuses the fastest (Caracas and Panero, 2017). Figure 2 shows OH bands converging to the high-wavenumber region at temperatures above 400 °C. The similar OH spectra pattern changing with temperature was also found in previous high-temperature experiments on an iron-bearing ringwoodite (Mrosko et al., 2013). The authors considered this change to the trivalent iron produced in the dehydrogenation process. Indeed, the 3425 cm^{-1} band was suggested to be hydrogen associated with tetrahedrally coordinated ferric iron (Thomson et al., 2021). Thus, the increase integral absorbance ratio of 3425 to 3215 cm^{-1} band in our study agrees with the interpretation of Mrosko et al. (2013). On the other hand, considering that multiple hydrogen defects exist in ringwoodite (Panero et al., 2013), and that this phenomenon occurs near the dehydrogenation temperature of 400 °C, the site-specific stabilities of hydrogen defects in ringwoodite may provide an interpretation as well.

In addition to temperature-induced re-distribution of hydrogen defects, O-H bonding strength is also modified with increasing temperature, which is reflected by the OH wavenumber evolutions with increasing temperature in Figure 7. For the wadsleyite, the 3583 cm^{-1} peak shifts moderately to lower wavenumbers with increasing temperature, suggesting temperature-induced weakening of O-H bonding. The wavenumber of 3583 cm^{-1} band does not change under compression (Yang et al., 2014), thus pressure may have little impact on O-H bonding strength corresponding to this OH band. The 3385 and 3335 cm^{-1} bands gently shift to higher wavenumbers first and then have turning points between 200-300 °C. The discontinuities are consistent with the temperature of hydrogen defects transferring proposed above. The wavenumber evolutions of the two bands with temperature are different from those with pressure. As shown in Yang et al. (2014), the two bands progressively shift to lower wavenumbers with increasing pressure without discontinuities. For the ringwoodite, the 3650 cm^{-1} band slightly shifts to lower wavenumbers with increasing temperature. In contrast, the 3425 and 3125 cm^{-1} peaks drastically shift to higher wavenumbers at temperatures above 200 °C. The high-wavenumber shifting of OH band with increasing temperature indicate weakening of hydrogen bonding rather than O-H bonding plays a part. The turning point at 200 °C for the 3425 and 3125 cm^{-1} bands occurs at a temperature lower than the dehydrogenation temperature. Therefore,

the discontinuity suggests the relative variation of O-H bonding to hydrogen bonding before dehydrogenation.

Hydrogen effects on the framework of the wadsleyite and ringwoodite at high temperature and high pressure

Based on the literature compilation of Raman modes of pure Mg wadsleyite at ambient condition (Yang et al., 2012), Figure 8a shows that the Raman modes generally shift to lower wavenumbers with increasing water content. In contrast to Fe-free wadsleyite, water seems to have an opposite effect on some Raman modes. Based on the limited reported data, hydrogen seems to have no effect on the Raman modes of Fe-free ringwoodite and Fe-bearing ringwoodite at ambient condition (Chopelas et al., 1994; Kleppe et al., 2002a, 2002b; Liu et al., 2002).

To track the Raman modes evolutions with temperature, wavenumbers of the main Raman modes of the wadsleyite and ringwoodite are plotted to temperatures under ambient pressure and high pressure, respectively (Figure 8b-c). For both wadsleyite and ringwoodite, the modes with wavenumbers higher than 400 cm^{-1}, related to Si-O polyhedron vibrations, shift linearly to lower wavenumbers with increasing temperature. But the shift amplitudes are different at ambient pressure and high pressure as shown in Table 1. For example, the shift amplitudes of the two representative modes of the wadsleyite with temperature at 14.27 GPa are smaller than those at ambient pressure. In contrast, the shift amplitudes of the two representative modes of the ringwoodite with temperature at 18.84 GPa are larger than those at ambient pressure. When the shift amplitudes of the Si-O polyhedron modes are compared between wadsleyite and ringwoodite, it can be found that temperature has a greater impact on the ringwoodite. This is consistent with the aforementioned greater pressure impact on the ringwoodite than the wadsleyite. This indicates that the Si-O polyhedron of ringwoodite may be more deformable than that of wadsleyite. On the other hand, for the modes with wavenumbers lower than 400 cm^{-1}, related to lattice vibrations, the discontinuities were observed for both wadsleyite and ringwoodite in Figure 8b-c. For example, with increasing temperature, the mode at 173 cm^{-1} of the wadsleyite slightly shifts to higher wavenumbers with increasing temperature to 600 °C, and then drastically shifts to higher wavenumbers. Similarly, the shifts of the modes at 211 cm^{-1} and 237 cm^{-1} of the ringwoodite display

the turning points at 200 °C. The discontinuities of the lattice modes shifting with temperature of the wadsleyite and ringwoodite are in accordant with the aforementioned dehydrogenation in the wadsleyite and hydrogen bonding modification of the ringwoodite. Therefore, dehydrogenation in wadsleyite and hydrogen bonding modification of ringwoodite at high temperatures are internally linked to the framework behavior.

In addition, considering that the mantle transition zone contains Fe and hydrogen, hydrogen and Fe impacts on the framework behavior of the two minerals at high temperature and high pressure should be evaluated. However, to date, there is only one report of Raman modes of the hydrous iron-free wadsleyite at simultaneously high temperature and high pressure (Yang et al., 2012). The main Raman modes of hydrous iron-bearing wadsleyite in our study changes less with temperature under high pressure compared with Yang et al. (2012), indicating a possible iron effect. So far, there has been no report on the Raman modes of hydrous iron-free ringwoodite at simultaneous high temperature and high pressure, thus, the effect of iron on the deformation of ringwoodite Si-O polyhedron still cannot be evaluated. In addition, there has been no reports of the Raman modes of anhydrous wadsleyite and ringwoodite at simultaneously high temperature and high pressure, thus hydrogen effect at simultaneous high temperature and high pressure cannot be revealed either. Alternatively, hydrogen and Fe effects at room temperature under high pressure or at high temperatures under ambient pressure could be estimated. It has been suggested that hydrogen and Fe have a minor effect on the framework behavior of ringwoodite under high pressures at room temperature (Kleppe et al., 2006). In contrast, hydrogen and Fe effects on the response of Si-O polyhedron of ringwoodite to temperature at ambient are evident in Figure 9 based on comparisons of available data. The responses of Si-O polyhedron to temperature are different between hydrous and anhydrous ringwoodite, and between Fe-free and Fe-bearing ringwoodite. Therefore, it may be inferred that hydrogen and Fe should impact the framework behavior of ringwoodite at simultaneous high temperature and high pressure relevant to the mantle transition zone. As shown in Figure 9, the Raman modes have a smaller shift amplitude with temperature for the hydrous ringwoodite than the anhydrous one, which may be responsible for the recent finding that water reduces the lattice thermal conductivity of ringwoodite (Marzotto et al., 2020).

IMPLICATIONS

This study experimentally revealed the hydrogen defect and framework behavior of the Fe-bearing wadsleyite and ringwoodite at high temperature and high pressure. The results provide new knowledge about hydrogen defects and framework of the two minerals, which is important for understanding water storage and physical properties of the mantle transition zone. It has been found that hydrous ringwoodite had a higher electrical conductivity than hydrous wadsleyite (e.g., Yoshino et al., 2008a). There are many possible reasons for this, such as hydrogen and Mg mobilities in the crystal structure, amounts of free protons, pressure conditions and crystal structures. The lower dehydrogenation temperature in ringwoodite than in wadsleyite here may suggest different hydrogen mobilities in the two minerals, thus providing experimental evidence for understanding the higher electrical conductivity of hydrous ringwoodite. Indeed, water loss at high temperatures has been proposed to be one of the reasons for the discrepancies in the electrical conductivities of wadsleyite (Yoshino and Katsura, 2012). Furthermore, it has been revealed for olivine that different hydrogen defects have different solubilities and impacts on physical properties (Faul et al., 2016; Padrón-Navarta and Hermann, 2017). The site-specific stabilities of hydrogen defects in wadsleyite and ringwoodite may provide new sight for further research on water solubility and impacts on properties of the two minerals. At last, based on lattice dynamics, the lattice vibrations are related to several properties such as thermal expansion, intrinsic elasticity and thermal conductivity. Our study revealed the effects of hydrogen and Fe on the framework behavior of the two minerals at high temperature and high pressure, thus calling for the studies on the thermal conductivity of hydrous Fe-bearing wadsleyite and ringwoodite, to further understand heat transport in the mantle.

ACKNOWLEDGMENTS

This work is supported by the National Natural Science Foundation of China (42172041, 41972038) and Fundamental Research Funds for the Central Universities (Grant K20210168). Sylvie Demouchy is warmly thanked for manuscript discussion. Suwen Qiu is thanked for the EPMA experiment.

REFERENCES

Bolfan-Casanova, N., Keppler, H., and Rubie, D.C. (2000) Water partitioning between nominally anhydrous minerals in the MgO-SiO_2-H_2O system up to 24 GPa: implications for the distribution of water in the Earth's mantle. Earth and Planetary Science Letters, 182, 209–221.

Bolfan-Casanova, N., Muñoz, M., McCammon, C., Deloule, E., and Ferot, A. (2012) Ferric iron and water incorporation in wadsleyite under hydrous and oxidizing conditions: A XANES, Mössbauer, and SIMS study. American Mineralogist, 97 (8-9), 1483–1493.

Caracas, R., and Panero, W.R. (2017) Hydrogen mobility in transition zone silicates. Progress in Earth and Planetary Science, 4: 9.

Chamorro, Pérez, E.M., Daniel, I., Chervin, J.C., Dumas, P., Bass, J.D., and Inoue, T. (2006) Synchrotron IR study of hydrous ringwoodite (γ-Mg_2SiO_4) up to 30 GPa. Physics and Chemistry of Minerals, 33, 502–510.

Chopelas, A., Boehler, R., and Ko, T. (1994) Thermodynamics and Behavior of γ-Mg_2SiO_4 at High Pressure: Implications for Mg_2SiO_4 Phase Equilibrium. Physics and Chemistry of Minerals, 21: 351–359.

Dai, L., and Karato, S. (2014) High and highly anisotropic electrical conductivity of the asthenosphere due to hydrogen diffusion in olivine. Earth and Planetary Science Letters, 408, 79–86.

Deon, F., Koch-Müller, M., Rhede, D., Gottschalk, M., Wirth, R., and Sylvia-Monique, T. (2010) Location and quantification of hydroxyl in wadsleyite: New insights. American Mineralogist, 95, 312–322.

Faul, U., Cline, C.J., David, E.C., Berry, A.J., and Jackson, I. (2016) Titanium-hydroxyl defect-controlled rheology of the Earth's upper mantle. Earth and Planetary Science Letters, 452, 227-237.

Fei, H., and Katsura, T. (2020) High water solubility of ringwoodite at mantle transition zone temperature. Earth and Planetary Science Letters, 531, 115987.

Fei, H., and Katsura, T. (2021) Water solubility in Fe-bearing wadsleyite at mantle transition zone temperatures. Geophysical Research Letters, 48, e2021GL092836.

Grüninger, H., Armstrong, K., Greim, D., Boffa, Ballaran, T., Frost, D.J., and Senker, J. (2017) Hidden Oceans? Unraveling the Structure of Hydrous Defects in the Earth's Deep Interior. Journal of the American Chemical Society, 139, 10499–10505.

Hae, R., Ohtani, E., Kubo, T., Koyama, T., and Utada, H. (2006) Hydrogen diffusivity in wadsleyite and water distribution in the mantle transition zone. Earth and

Planetary Science Letters, 243(1–2), 141–148.

Huang, X., Xu, Y., and Karato, S.I. (2005) Water content in the transition zone from electrical conductivity of wadsleyite and ringwoodite. Nature, 434, 746–749.

Houser, C. (2016) Global seismic data reveal little water in the mantle transition zone. Earth and Planetary Science Letters, 448, 94–101.

Inoue, T., Tanimoto, Y., Irifune, T., Suzuki, T., Fukui, H., and Ohtaka, O. (2004) Thermal expansion of wadsleyite, ringwoodite, hydrous wadsleyite and hydrous ringwoodite. Physics of the Earth and Planetary Interiors, 143–144, 279–290.

Jacobsen, S.D., Demouchy, S., Frost, D.J., Ballaran, T.B., and Kung, J. (2005) A systematic study of OH in hydrous wadsleyite from polarized FTIR spectroscopy and single-crystal X-ray diffraction: Oxygen sites for hydrogen storage in Earth's interior. American Mineralogist, 90, 61–70.

Jollands, M. C., Kempf, E., Hermann, J., and Müntener, O. (2019) Coupled inter-site reaction and diffusion: Rapid dehydrogenation of silicon vacancies in natural olivine. Geochimica et Cosmochimica Acta, 262, 220-242.

Kleppe, A.K., Jephcoat, A.P., Olijnyk, H., Slesinger, A.E., Kohn, S.C., and Wood, B.J. (2001) Raman spectroscopic study of hydrous wadsleyite (β-Mg_2SiO_4) to 50 GPa. Physics and Chemistry of Minerals, 28, 232–241.

Kleppe, A.K., Jephcoat, A.P., and Smyth, J.R. (2002a) Raman spectroscopic study of hydrous γ-Mg_2SiO_4 to 56.5 GPa. Physics and Chemistry of Minerals, 29, 473–476.

Kleppe, A.K., Jephcoat, A.P., Smyth, J.R., and Frost, D.J. (2002b) On protons, iron and the high-pressure behavior of ringwoodite. Geophysical Research Letter, 29(21), 17-1–17-4.

Kleppe, A.K., Jephcoat, A.P., and Smyth, J.R. (2006) High-pressure Raman spectroscopic study of Fo_{90} hydrous wadsleyite. Physics and Chemistry of Minerals, 32, 700–709.

Koch-Müller, M., Speziale, S., Deon, F., Mrosko, M., and Schade, U. (2011) Stress-induced proton disorder in hydrous ringwoodite. Physics and Chemistry of Minerals, 38, 65–73.

Kohlstedt D.L., Keppler, H., and Rubie, D.C. (1996) Solubility of water in the α, β, and γ phases of $(Mg, Fe)_2SiO_4$. Contributions to Mineralogy and Petrology, 123, 345–357.

Kohn, S.C., Brooker, R.A., Frost, D.J., Slesinger, A.E., and Wood, B.J. (2002) Ordering of hydroxyl defects in hydrous wadsleyite (β-Mg_2SiO_4). American Mineralogist, 87, 293–301.

Liu, L.-G., Mernagh, T.P., Lin, C.-C., and Inoue, T. (1998) Raman Spectra of Hydrous

β-Mg2SiO4 at Various Pressures and Temperatures. in: Properties of Earth and Planetary Materials at High Pressure and Temperature, 101, edited by: Manghnani, M.H., Yagi, T., American Geophysical Union, Washington, D.C., 523–530.

Liu, L., Mernagh, T.P., Lin, C.-C., and Inoue, T. (2002) Raman spectra of γ-Mg_2SiO_4 at various pressures and temperatures. Physics and Chemistry of Minerals, 29, 181–187.

Mao, H.K., Xu, J., and Bell, P.M. (1986) Calibration of the ruby pressure gauge to 800 kbar under quasi-hydrostatic conditions. Journal of Geophysical Research, 91, 4763–4767.

Marzotto, E., Hsieh, W., Ishii, T., Chao, K., Golabek, G.J., Thielmann, M., and Ohtani, E. (2020) Effect of water on lattice thermal conductivity of ringwoodite and its implications for the thermal evolution of descending slabs. Geophysical Research Letters, 47(13).

Mernagh, T.P., and Liu, L.G. (1996) Raman and infrared spectra of hydrous b-Mg2SiO4. Canadian Mineralogist, 34, 1233–1240.

Mrosko, M., Lenz, S., McCammon, C.A., Taran, M., Wirth, R., and Koch-Müller, M. (2013) Hydrogen incorporation and the oxidation state of iron in ringwoodite: A spectroscopic study. American Mineralogist, 98(4), 629–636.

Padro´n-Navarta, J.A., and Hermann, J. (2017) A subsolidus olivine water solubility equation for the earth's upper mantle. Journal of Geophysical Research: Solid Earth, 122, 9862–9880.

Panero, W.R., Smyth, J.R., Pigott, J.S., Liu Z., and Frost, D.J. (2013) Hydrous ringwoodite to 5 K and 35 GPa: Multiple hydrogen bonding sites resolved with FTIR spectroscopy. American Mineralogist, 98, 637–642.

Pearson, D.G., Brenker, F.E., Nestola, F., McNeill, J., Nasdala, L., Hutchison, M.T., Matveev, S., Mather, K., Silversmit, G., Schmitz, S., Vekemans, B., and Vincze, L. (2014) Hydrous mantle transition zone indicated by ringwoodite included within diamond. Nature, 507, 221–224.

Rekhi, S., Dubrovinsky, L.S., and Saxena, S.K. (1999) Temperature-induced ruby fluorescence shifts up to a pressure of 15 GPa in an externally heated diamond anvil cell. High Temp High Press, 31, 299–305.

Smyth, J.R. (1994) A crystallographic model for hydrous wadsleyite (b-Mg_2SiO_4): an ocean in the Earth's interior? American Mineralogist, 79, 1021–1024.

Sun, W., Yoshino, T., Sakamoto, N., and Yurimoto, H. (2015) Hydrogen self-diffusivity in single crystal ringwoodite: Implications for water content and distribution in the mantle transition zone. Geophysical Research Letters, 42, 6582–6589.

Sun, W., Yoshino, T., Sakamoto, N., and Yurimoto, H. (2018) Supercritical fluid in the mantle transition zone deduced from H–D interdiffusion of wadsleyite. Earth and Planetary Science Letters, 484, 309–317.

Thomson, A.R., Piltz, R.O., Crichton, W.A., Cerantola, V., Ezad, I.S., Dobson, D.P., Wood, I.G., and Brodholt, J.P. (2021) Incorporation of tetrahedral ferric iron into hydrous ringwoodite. American Mineralogist, 106, 900–908.

Yang, X., Dubrovinsky, L., Manthilake, M.A.G.M., and Wei, Q. (2012) High-pressure and high-temperature Raman spectroscopic study of hydrous wadsleyite (β-Mg_2SiO_4). Physics and Chemistry of Minerals, 39, 57–64.

Yang, X., Keppler, H., Dubrovinsky, L., and Kurnosov, A. (2014) In-situ infrared spectra of hydroxyl in wadsleyite and ringwoodite at high pressure and high temperature. American Mineralogist, 99, 724–729.

Ye, Y., Schwering, R.A., and Smyth, J.R. (2009) Effect of hydration on thermal expansion of forsterite, wadsleyite and ringwoodite at ambient pressure. American Mineralogist, 94, 899–904.

Ye, Y., Smyth, J.R., and Frost, D.J. (2011) Structural study of the coherent dehydration of wadsleyite. American Mineralogist, 96, 1760–1767.

Ye, Y., Brown, D.A., Smyth, J.R., Panero, W.R., Jacobsen, S.D., Chang, Y.Y., Townsend J.P., Thomas, S.-M., Hauri, E.H., Dera, P., and Frost, D.J. (2012) Compressibility and thermal expansion of hydrous ringwoodite with 2.5(3) wt% H_2O. American Mineralogist, 97, 573–582.

Yoshino, T., Manthilake, G., Matsuzaki, T., and Katsura, T. (2008a) Dry mantle transition zone inferred from electrical conductivity of wadsleyite and ringwoodite. Nature, 451, 326–329.

Yoshino, T., Nishi, M., Matsuzaki, T., Yamazaki, D., and Katsura, T. (2008b) Electrical conductivity of majorite garnet and its implications for electrical structure in the mantle transition zone. Physics of the Earth and Planetary Interiors, 170, 193–200.

Yoshino, T., and Katsura, T. (2012) Re-evaluation of electrical conductivity of anhydrous and hydrous wadsleyite. Earth and Planetary Science Letters, 337–338, 56–67.

Zhang, B., and Xia, Q. (2021) Influence of water on the physical properties of olivine, wadsleyite, and ringwoodite. European Journal of Mineralogy, 33, 1–37.

Zhou, W.Y., Mao, M., Zhang, J.S., Chen, B., Wang, R.J., and Schmandt, B. (2022) Constraining composition and temperature variations in the mantle transition zone. Nature Communications, 13, 1094.

Table 1 Evolutions of the representative Raman modes with temperature at ambient pressure and high pressure. The data in italic are standard error

Wadsleyite			Ringwoodite		
Raman mode/cm^{-1}	(dν/dt)/ ($cm^{-1}\cdot°C^{-1}$)	Pressure/GPa	Raman mode/cm^{-1}	(dν/dt)/ ($cm^{-1}\cdot°C^{-1}$)	Pressure/GPa
760	-0.00940 *0.00194*	14.27	874	-0.04168 *0.00779*	18.84
967	-0.01153 *0.00303*	14.27	900	-0.02097 *0.00282*	18.84
720	-0.01711 *0.00123*	0	797	-0.03439 *0.00242*	0
918	-0.01957 *0.00162*	0	838	-0.00807 *0.00380*	0

Figure captions

Figure 1 FTIR spectra of hydrogen defects at ambient condition: (a) Polarized spectra for wadsleyite. X' and Y' indicates that the polarizer was rotated to vertical angels; (b) Unpolarized spectra for ringwoodite

Figure 2 (a)-(c) *In situ* FTIR spectra of hydrogen defects at high temperatures. X' and Y' indicates that the polarizer was rotated to vertical angels. (d)-(f) FTIR spectra of hydrogen defects at room temperature of the samples quenched from high temperatures

Figure 3 Raman spectra of the two samples at ambient condition

Figure 4 *In situ* Raman spectra at different temperatures of the two samples: (a-b) At ambient pressure; (c-d) Under high pressure

Figure 5 Variations of the bulk integral absorbance (Ab) with temperature: (a) Wadsleyite; (b) Ringwoodite

Figure 6 Integral absorbance ratio between OH bands versus temperature: (a) Wadsleyite; (b) Ringwoodite. The data are based on the *in situ* high-temperature FTIR spectra.

Figure 7 OH wavenumber versus temperature: (a) Wadsleyite; (b) Ringwoodite. The data are based on the *in situ* high-temperature FTIR spectra.

Figure 8 (a) Relationships between Raman modes and water contents for wadsleyite. The data for wadsleyite of Fo100 are from Chopelas (1991); Kleppe et al. (2001); Liu et al. (1994, 1998); McMillan et al. (1991); Yang et al. (2012). The data for wadsleyite of Fo90 are from Kleppe et al. (2006) and this study; (b) Evolutions of Raman modes of wadsleyite with temperature at ambient pressure (solid

symbols) and high pressure (open symbols); (c) Evolutions of Raman modes of ringwoodite with temperature at ambient pressure (solid symbols) and high pressure (open symbols)

Figure 9 Comparison of the two Si-O polyhedron modes of ringwoodite with different water and Fe contents

Figure 1

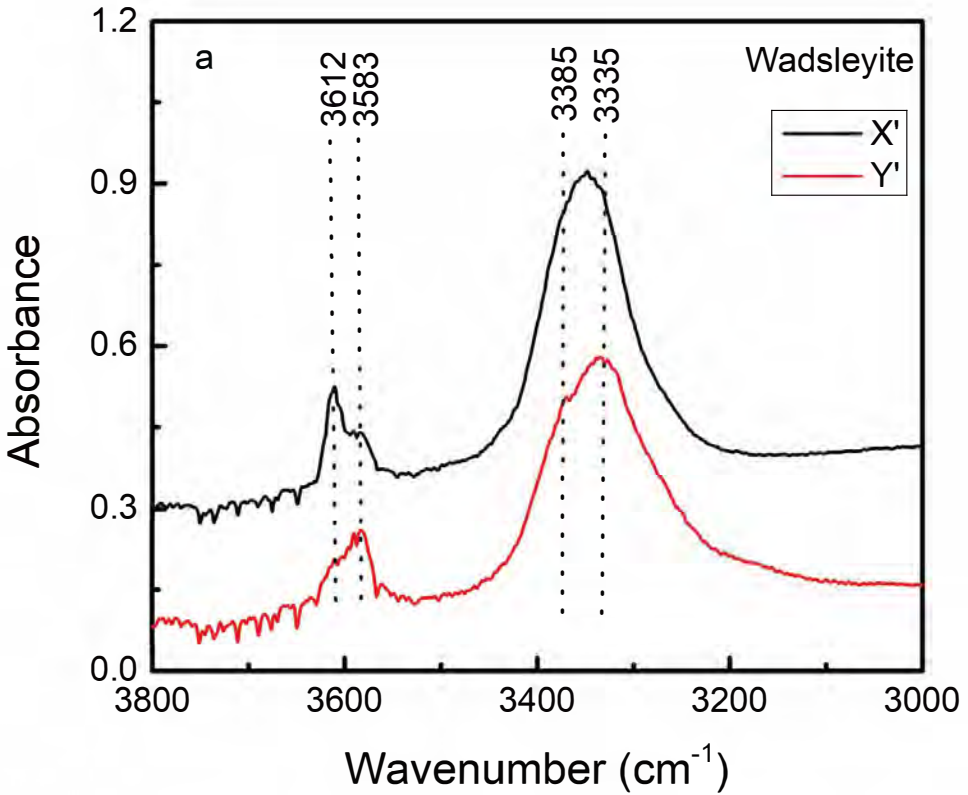
a
Wadsleyite
X'
Y'
3612
3583
3385
3335
Absorbance
Wavenumber (cm-1)
1.2
0.9
0.6
0.3
0.0
3800
3600
3400
3200
3000

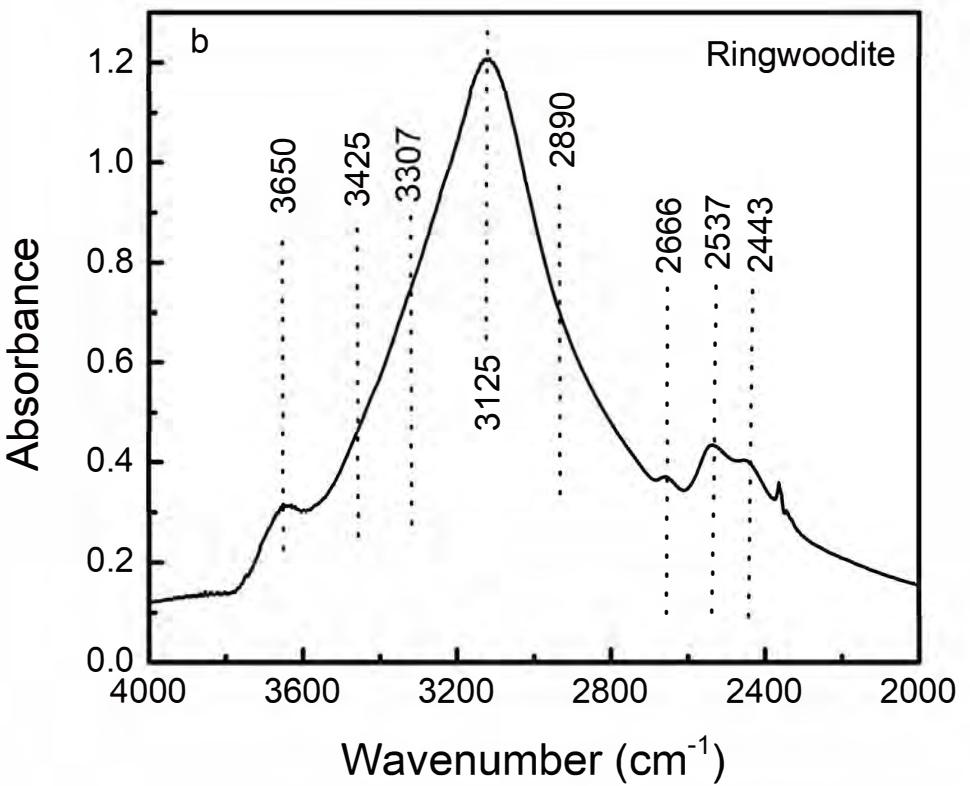
b
Ringwoodite
3650
3425
3307
3125
2890
2666
2537
2443
Absorbance
Wavenumber (cm-1)
1.2
1.0
0.8
0.6
0.4
0.2
0.0
4000
3600
3200
2800
2400
2000

Figure 2

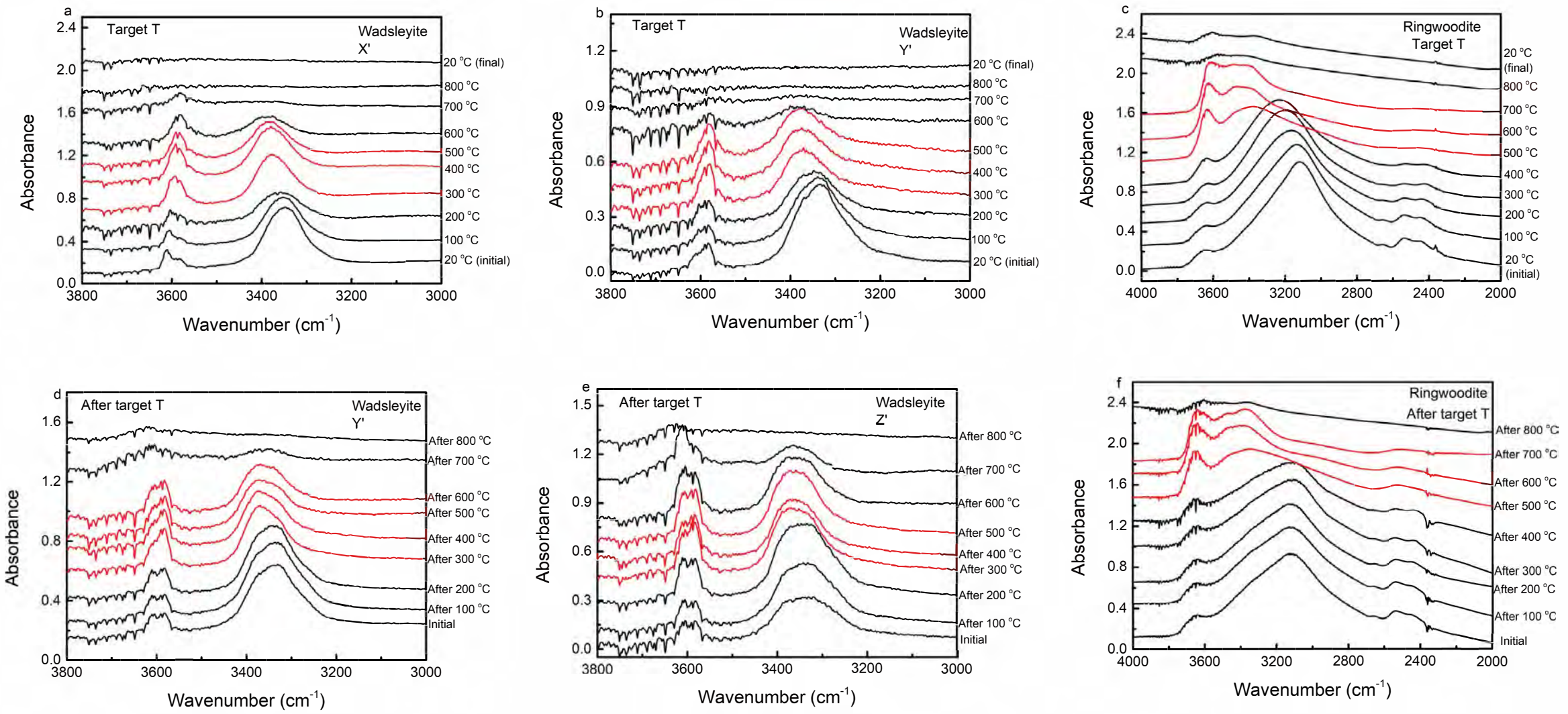
a
Target T
Wadsleyite X'
20 °C (final)
800 °C
700 °C
600 °C
500 °C
400 °C
300 °C
200 °C
100 °C
20 °C (initial)
Absorbance
Wavenumber (cm-1)
b
Target T
Wadsleyite Y'
20 °C (final)
800 °C
700 °C
600 °C
500 °C
400 °C
300 °C
200 °C
100 °C
20 °C (initial)
Absorbance
Wavenumber (cm-1)
c
Ringwoodite Target T
20 °C (final)
800 °C
700 °C
600 °C
500 °C
400 °C
300 °C
200 °C
100 °C
20 °C (initial)
Absorbance
Wavenumber (cm-1)
d
After target T
Wadsleyite Y'
After 800 °C
After 700 °C
After 600 °C
After 500 °C
After 400 °C
After 300 °C
After 200 °C
After 100 °C
Initial
Absorbance
Wavenumber (cm-1)
e
After target T
Wadsleyite Z'
After 800 °C
After 700 °C
After 600 °C
After 500 °C
After 400 °C
After 300 °C
After 200 °C
After 100 °C
Initial
Absorbance
Wavenumber (cm-1)
f
Ringwoodite After target T
After 800 °C
After 700 °C
After 600 °C
After 500 °C
After 400 °C
After 300 °C
After 200 °C
After 100 °C
Initial
Absorbance
Wavenumber (cm-1)

Figure 3

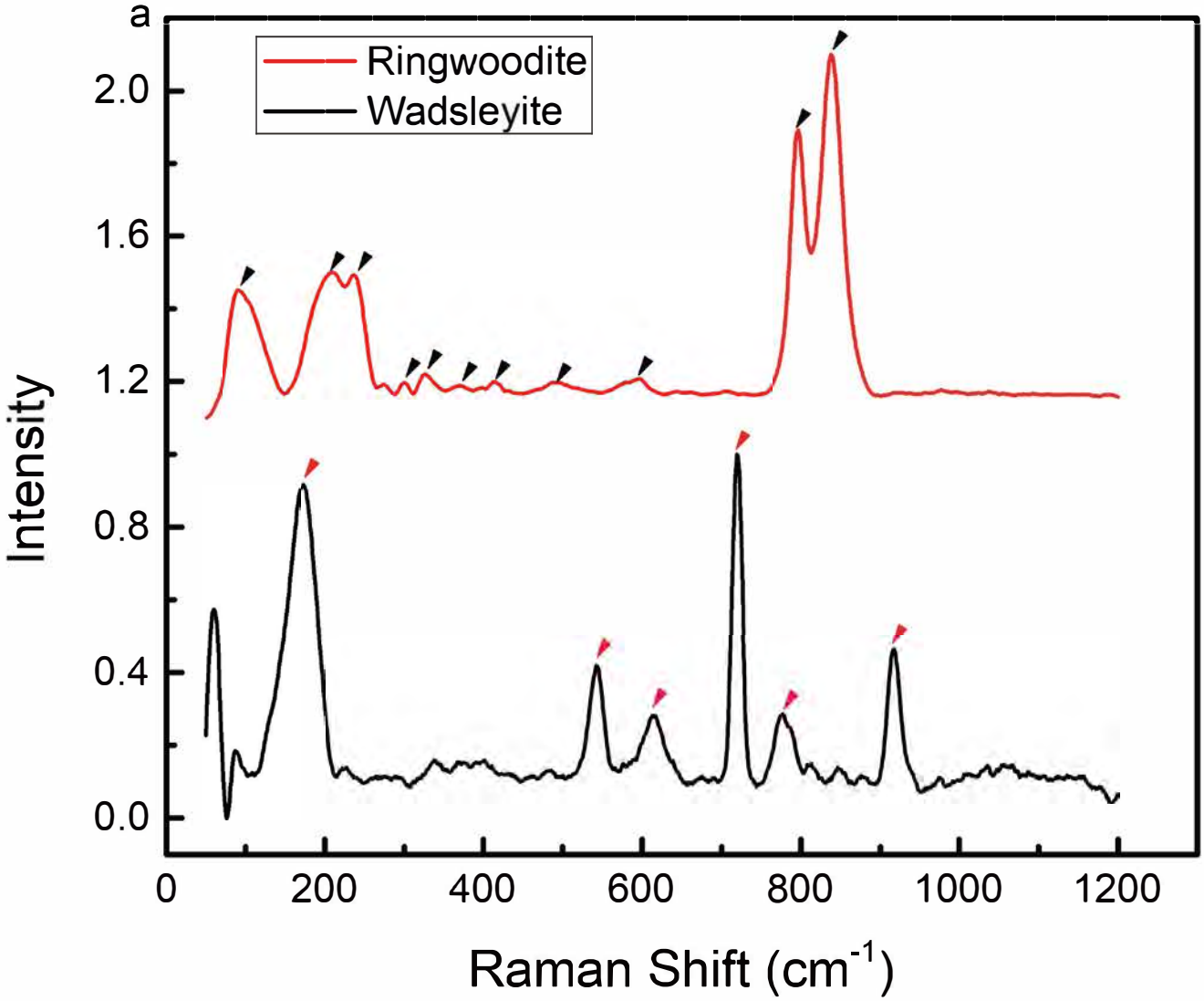
a
Ringwoodite
Wadsleyite
Intensity
2.0
1.6
1.2
0.8
0.4
0.0
0
200
400
600
800
1000
1200
Raman Shift (cm-1)

Figure 4

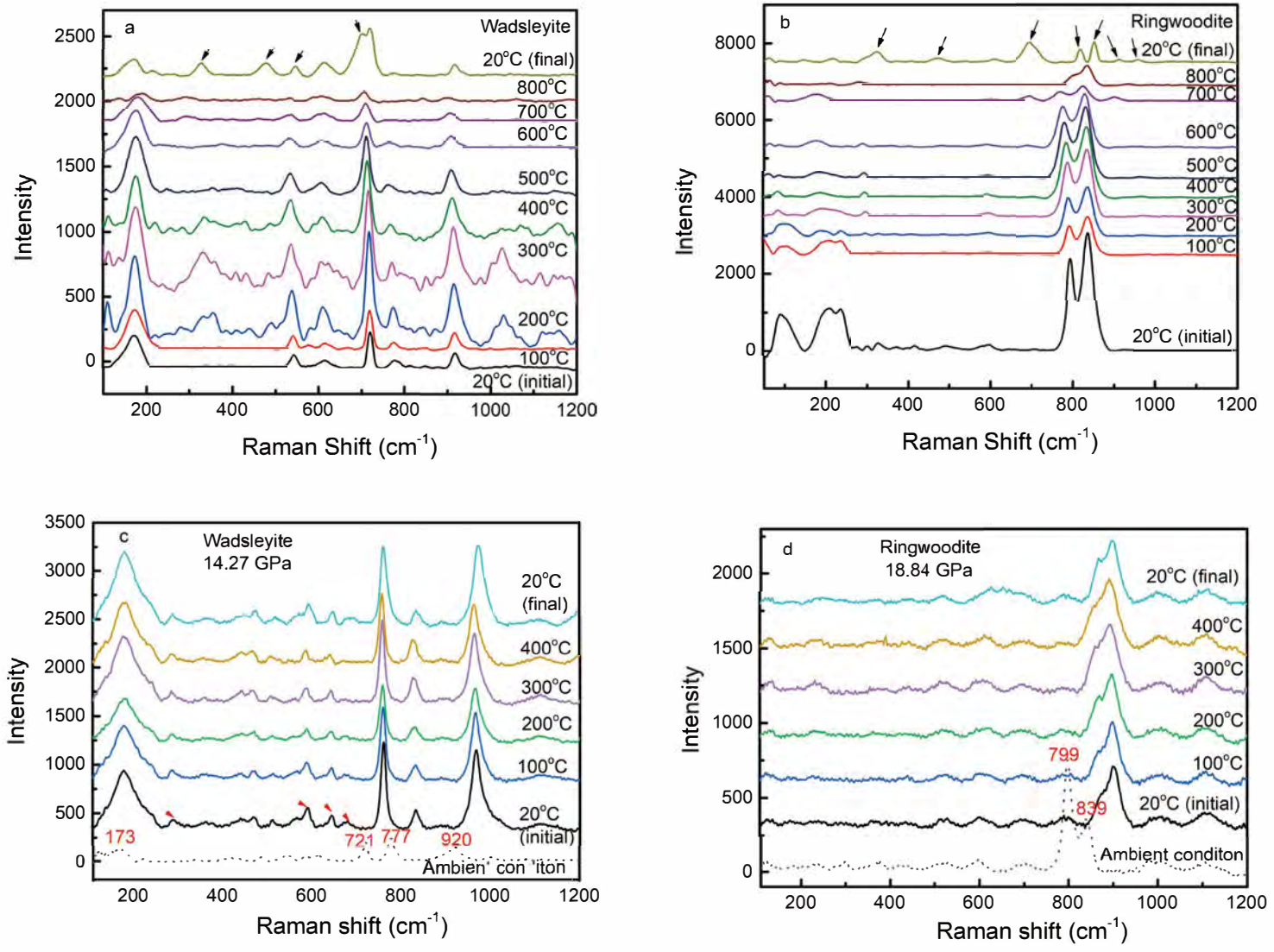
a
Wadsleyite
20°C (final)
800°C
700°C
600°C
500°C
400°C
300°C
200°C
100°C
20°C (initial)
Intensity
Raman Shift (cm-1)
b
Ringwoodite
20°C (final)
800°C
700°C
600°C
500°C
400°C
300°C
200°C
100°C
20°C (initial)
Intensity
Raman Shift (cm-1)
c
Wadsleyite
14.27 GPa
20°C (final)
400°C
300°C
200°C
100°C
20°C (initial)
173
721
777
920
Ambien con iton
Intensity
Raman shift (cm-1)
d
Ringwoodite
18.84 GPa
20°C (final)
400°C
300°C
200°C
100°C
20°C (initial)
799
839
Ambient conditon
Intensity
Raman shift (cm-1)

Figure 5

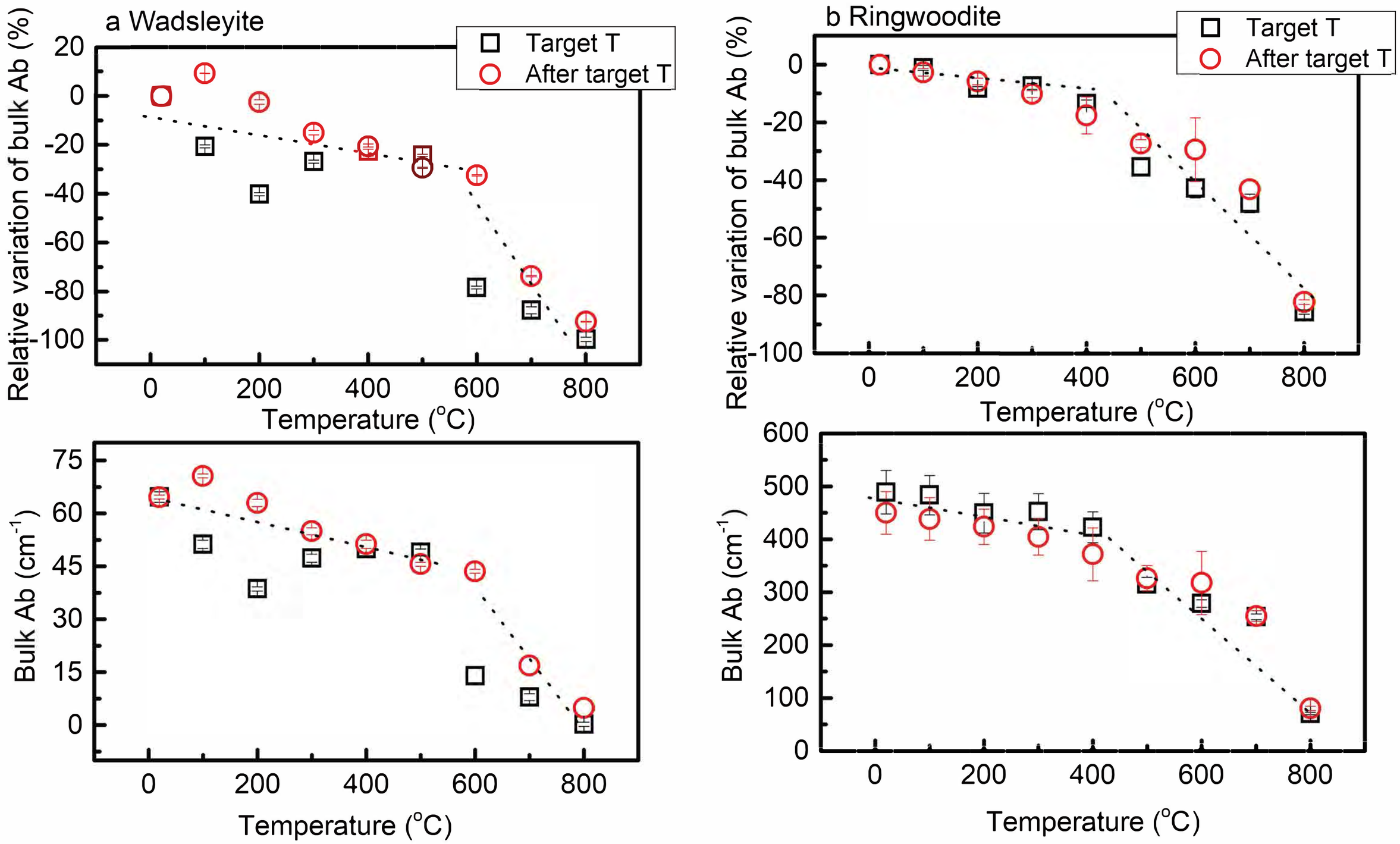
a Wadsleyite
b Ringwoodite
Target T
After target T
Relative variation of bulk Ab (%)
Bulk Ab (cm^{-1})
Temperature (°C)
20
0
-20
-40
-60
-80
-100
75
60
45
30
15
0
200
400
600
800

Figure 6

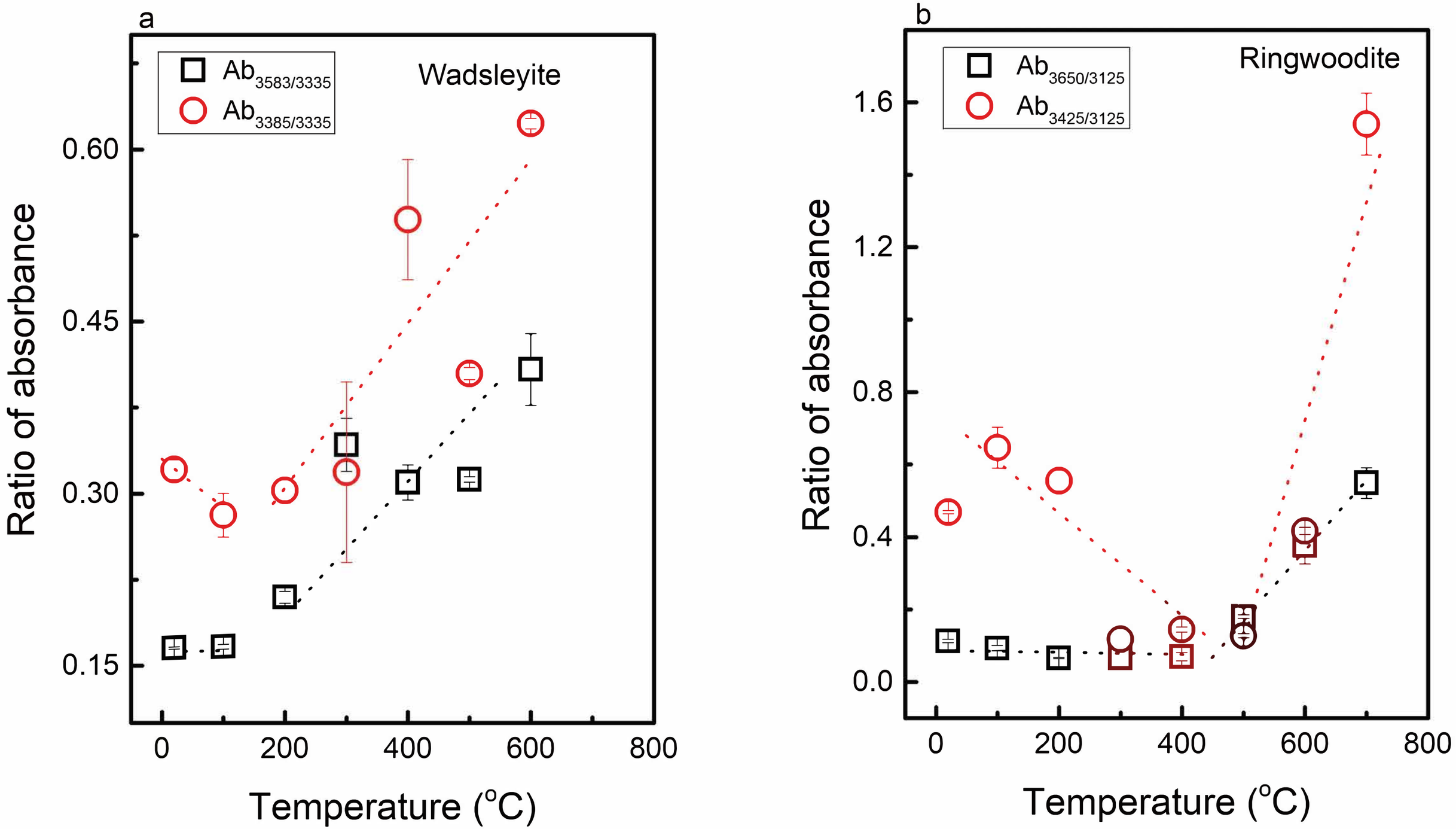
a
Wadsleyite
Ab3583/3335
Ab3385/3335
Ratio of absorbance
0.60
0.45
0.30
0.15
0
200
400
600
800
Temperature (°C)
b
Ringwoodite
Ab3650/3125
Ab3425/3125
Ratio of absorbance
1.6
1.2
0.8
0.4
0.0
0
200
400
600
800
Temperature (°C)

Figure 7

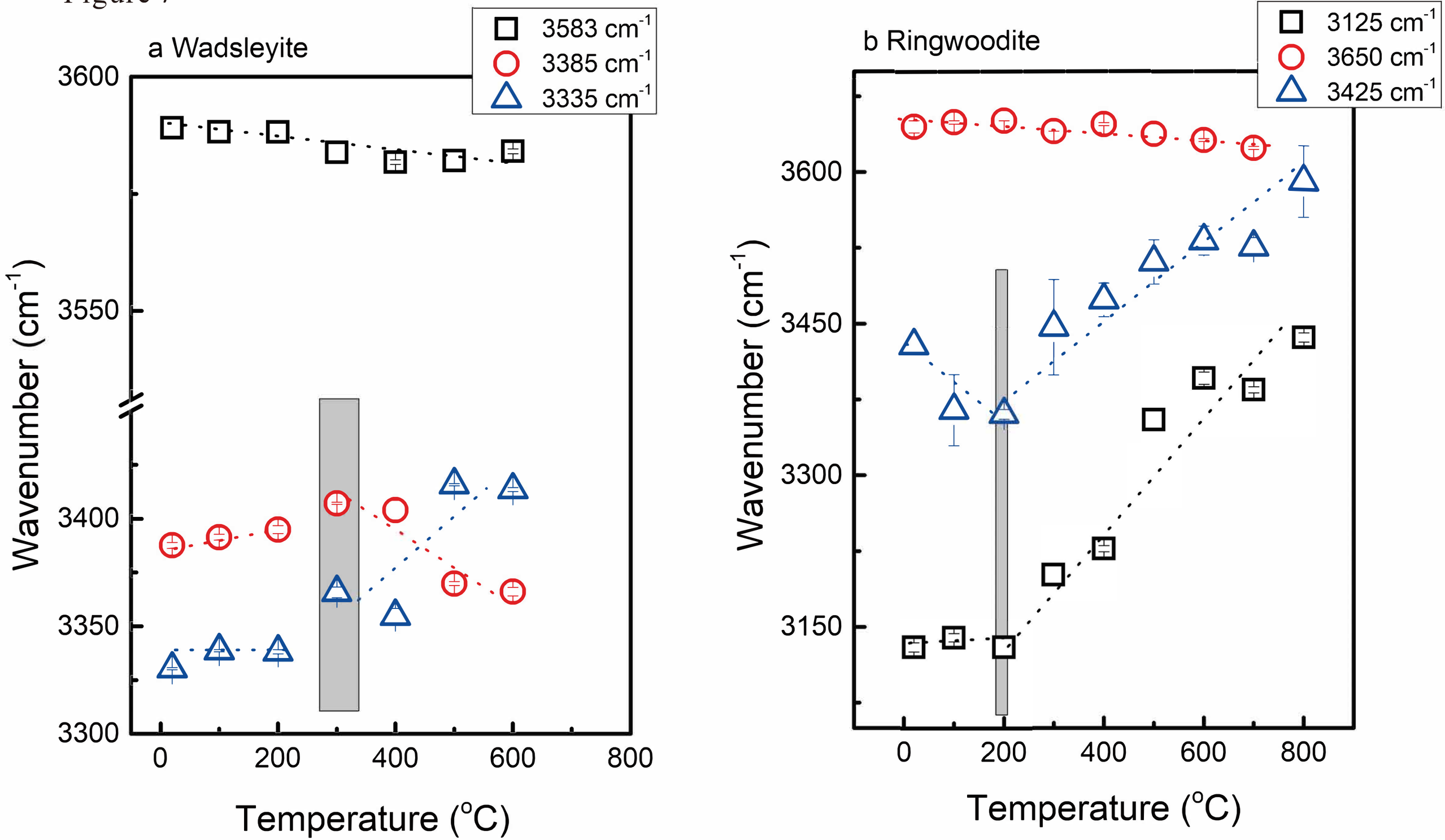
a Wadsleyite
3583 cm-1
3385 cm-1
3335 cm-1
Wavenumber (cm-1)
3600
3550
3400
3350
3300
0
200
400
600
800
Temperature (°C)
b Ringwoodite
3125 cm-1
3650 cm-1
3425 cm-1
Wavenumber (cm-1)
3600
3450
3300
3150
0
200
400
600
800
Temperature (°C)

Figure 8

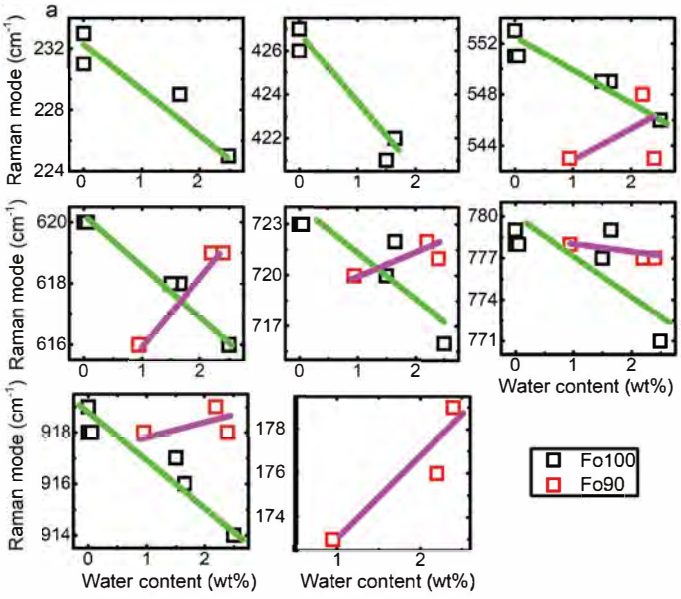
a
Raman mode (cm-1)
Water content (wt%)
Fo100
Fo90

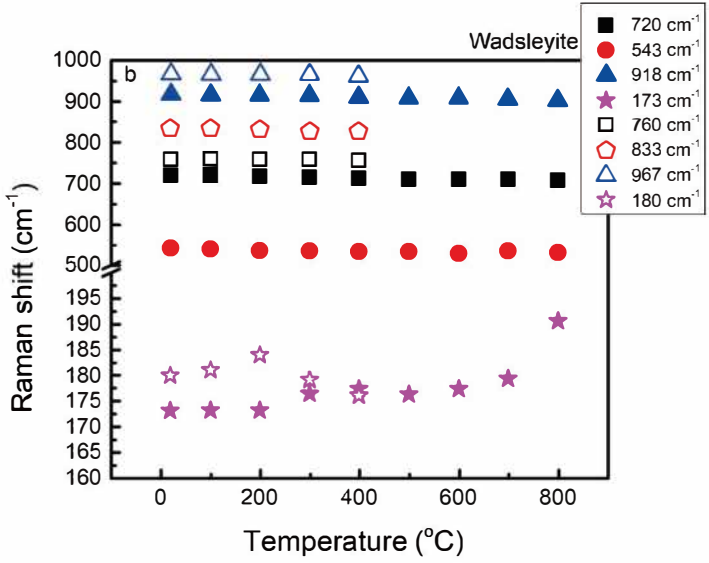
Wadsleyite
b
720 cm-1
543 cm-1
918 cm-1
173 cm-1
760 cm-1
833 cm-1
967 cm-1
180 cm-1
Raman shift (cm-1)
Temperature (°C)

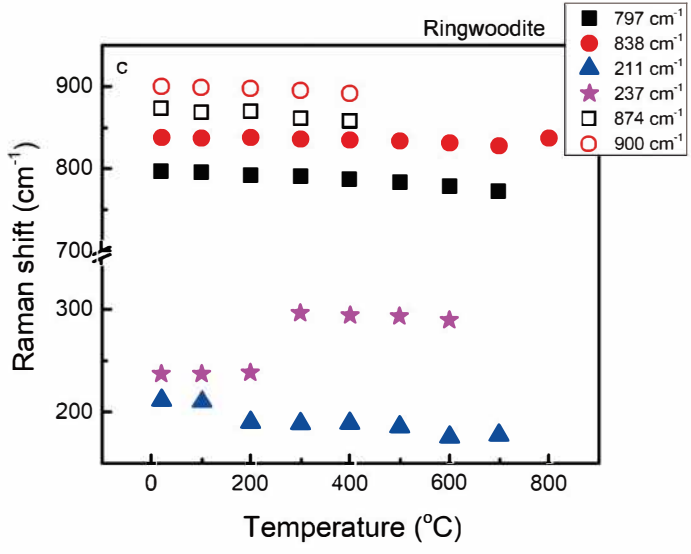
Ringwoodite
c
797 cm-1
838 cm-1
211 cm-1
237 cm-1
874 cm-1
900 cm-1
Raman shift (cm-1)
Temperature (°C)

Figure 9

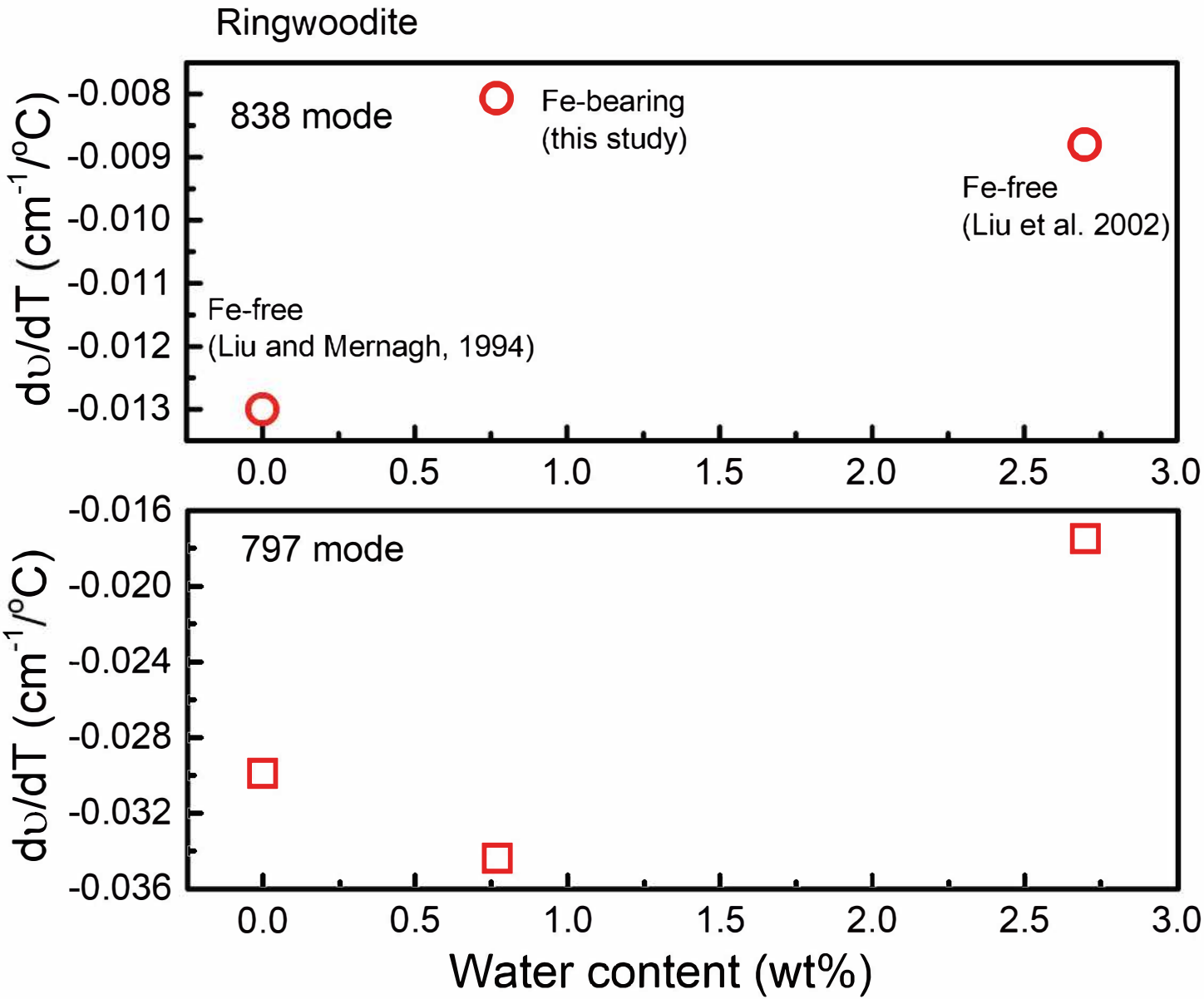
Ringwoodite
838 mode
Fe-bearing
(this study)
Fe-free
(Liu et al. 2002)
Fe-free
(Liu and Mernagh, 1994)
dυ/dT (cm-1/°C)
-0.008
-0.009
-0.010
-0.011
-0.012
-0.013
0.0
0.5
1.0
1.5
2.0
2.5
3.0
797 mode
-0.016
-0.020
-0.024
-0.028
-0.032
-0.036
Water content (wt%)